



OPEN ACCESS

EDITED BY

Fuyin Ma,
Xi'an Jiaotong University, China

REVIEWED BY

Xiaofei Lyu,
Tianjin University, China
Nansha Gao,
Northwestern Polytechnical University,
China

*CORRESPONDENCE

Xiao Liang,
liangxiao@xtu.edu.cn
Liang Su,
suliang@xtu.edu.cn

SPECIALTY SECTION

This article was submitted to
Metamaterials,
a section of the journal
Frontiers in Materials

RECEIVED 09 June 2022

ACCEPTED 27 June 2022

PUBLISHED 22 July 2022

CITATION

Huang M, Liang X, Su L, He X, Li D, Chu J,
Wang S, Liang H and Zhang Y (2022),
The numerical analysis of the acoustic
streaming effect of a cavity acoustic
black hole.
Front. Mater. 9:965260.
doi: 10.3389/fmats.2022.965260

COPYRIGHT

© 2022 Huang, Liang, Su, He, Li, Chu,
Wang, Liang and Zhang. This is an open-
access article distributed under the
terms of the [Creative Commons
Attribution License \(CC BY\)](https://creativecommons.org/licenses/by/4.0/). The use,
distribution or reproduction in other
forums is permitted, provided the
original author(s) and the copyright
owner(s) are credited and that the
original publication in this journal is
cited, in accordance with accepted
academic practice. No use, distribution
or reproduction is permitted which does
not comply with these terms.

The numerical analysis of the acoustic streaming effect of a cavity acoustic black hole

Meilian Huang^{1,2}, Xiao Liang^{1,2*}, Liang Su^{1,2*}, Xingyun He³,
Danni Li², Jiaming Chu², Shengsheng Wang², Haofeng Liang²
and Yongyan Zhang⁴

¹Foshan Green Intelligent Manufacturing Research Institute of Xiangtan University, Foshan, China, ²Xiangtan University School of Mechanical Engineering, Xiangtan, China, ³Jianglu Electromechanical Group Co., Ltd., Xiangtan, China, ⁴School of Mechanical Engineering, Xi'an Polytechnic University, Xi'an, China

In this study, we use numerical methods to study the acoustic streaming effect of the acoustic black hole (ABH). Firstly, we build an ABH model to study the acoustic streaming effect. By deriving the waves equations and solving the Navier–Stokes equations, we obtain the flow field, sound field, and temperature field under the acoustic excitation. Secondly, the simulation result reveals the mechanism of acoustic streaming effects on the sound transmission characteristics of cavity ABH. The numerical results show that the abrupt decrease in the sound pressure is caused by the great changes in the velocity gradient caused by the catastrophe of cross section. The energy of the sound waves can also be dissipated by the thermal viscous layer at low frequencies. Finally, based on the acoustic streaming effects of the acoustic medium in the ABH, we propose feasible methods to enhance the sound insulation. Increasing the cross section of the cavity in ABH can get a better sound insulation effect at high frequencies, and decreasing the cross section can improve Sound Transmission Loss (STL). Through optimization, STL can reach more than 25 dB at low frequencies.

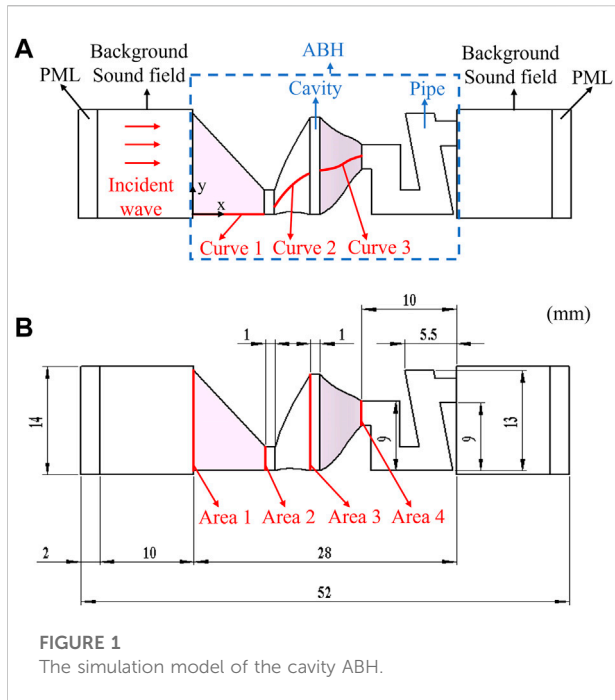
KEYWORDS

cavity acoustic black hole, acoustic streaming effects, acoustic transmission mechanism, sound insulation, numerical analysis

1 Introduction

Designing an acoustic black hole (ABH) structure is a method to suppress the sound waves (Denis et al., 2016; Gao et al., 2020; Gao and Lu, 2020). A flexural wave propagating in a power-law wedge at the end of a beam would progressively slow down and concentrate the wave energy at the tip of the wedge, which is affected by ABH (Mironov, 1988; Ma et al., 2021; Gao et al., 2022; Ma et al., 2022). In contrast, a small truncation end thickness at the tip of ABH can break the ABH effect, especially for low-frequency sound waves (Gao et al., 2019; Gao et al., 2021a; Gao et al., 2021b).

The ABH has attracted many researchers' attention. They analyzed the effects of defects at the truncated thickness to find ways to decrease the effect. One popular way is to add the



nonlinear geometry into the ABH, which can enhance the ABH effect (Denis et al., 2017; Li et al., 2019). The nonlinear geometry causes the energy cascade and wave turbulence, which can transfer energy from low frequency to high frequency to reduce the cut-off frequency and enlarge the ABH effect frequency range. It can improve the global passive vibration and sound radiation mitigation characteristics (Denis et al., 2017; Li et al., 2021).

Another popular way is to use the cavity ABH structure. One cavity ABH is called a sonic black hole (SBH), which is a series of rings with a power-law decaying inner radius installed in a duct. When the end is open, the Sound Transmission Loss (STL) at high frequency can reach more than 30 dB and even has good

sound absorption performance. However, there is a large reflection at low frequency, and the STL is also lower than 10 dB (Mi et al., 2021; Zhang and Cheng, 2021). Many studies have been conducted on sound absorption and insulation in view of acoustics. Many cavity ABH structures have been designed to achieve a better sound insulation effect (Mironov and Pisyakov, 2002; EI-Ouahabi et al., 2015a; EI-Ouahabi et al., 2015b; Mironov and Pisyakov, 2020). Xiao Liang purposed a comparatively large model of ABH and calculated the flow field in the cavity. Results reveal that the turbulence of the acoustic medium affects the acoustic transmission mechanism and illustrate that the acoustic streaming effects decide the acoustic transmission characteristics (Liang et al., 2019; Liang et al., 2021a; Liang et al., 2021b; Liang et al., 2022). Inspired by those excellent jobs, we proposed a cavity ABH to analyze its acoustic streaming effects and the sound transmission mechanism. In the study, we deeply explore the relationship between the acoustic streaming effects and the sound transmission mechanism, which has been rarely researched.

In this study, we propose a numerical simulation model and derive the governing equations. We get the flow, sound, and temperature fields by solving the governing equations in Section 2. In Section 3, by analyzing the numerical results, we explore the influence of streaming effects on the acoustic characteristics of the cavity ABH. By studying the flow, sound, and temperature fields, we discuss the relation between the acoustic streaming effects and the sound field. The conclusion is given in Section 4.

2 Numerical simulation model

2.1 Geometric model

A numerical simulation model is established to study the acoustic streaming effect and sound transmission mechanism of cavity ABH, as shown in Figure 1A. The spatial shape can be

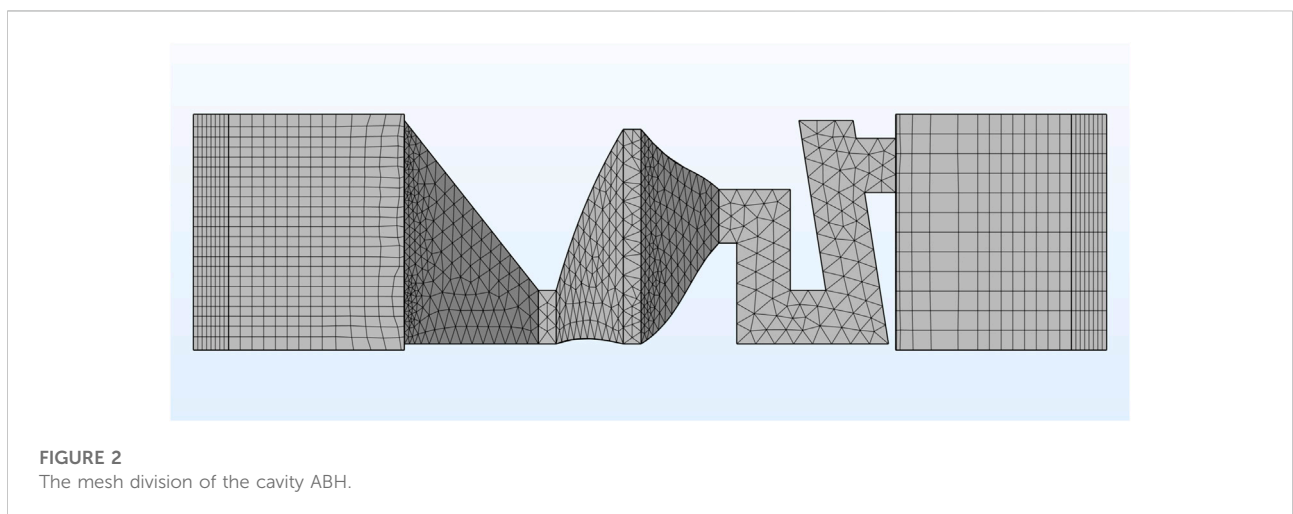


TABLE 1 The equations of the curves.

Line	Interval	Equations
Curve 1	$x \in (0, 7.5)$	$y = 0$
Curve 2	$x \in (8.5, 12.5)$	$y = 0.3997x^3 - 3.1578x^2 + 8.6866x - 7.3046$
Curve 3	$x \in (13.5, 18)$	$y = -0.6964x^4 + 7.329x^3 - 27.544x^2 + 42.983x - 21.323$

swept by two planes and a curve between the two planes. By using Curve 1, Curve 2, Curve 3, Area 1, Area 2, Area 3, and Area 4, the complex spatial shape of ABH can be formed. The specific equations of the curves are shown in Table 1. The detailed geometrical structure parameters of the cavity ABH are defined in Figure 1B. The overall length of ABH is 28 mm. The perfect match layer (PML) and the background sound field are symmetrical in the model. The lengths of the PML and the background sound field are 2 and 10 mm, respectively. The length between Area 1 and Area 2 is 7.5 mm. The shape of Area 1 and Area 2 is 12.7×25.4 mm and 3×3 mm rectangles, respectively. The length of the cavity is 9.5 mm, and the biggest section in the cavity is Area 3, a 22.9×12.2 mm rectangle. The pipe is 10 mm long; it has a section of 3×3 mm rectangle. The rest of the sizes are performed in Figure 1B.

The schematic diagram of the mesh division of the cavity ABH model is shown in Figure 2. We use a tetrahedron element to mesh the ABH model and use a triangle element to link up the background sound field and the ABH model. Then, we sweep the background sound field and the PML by Tetrahedral mesh. To ensure the accuracy of the simulation, we set the mesh division of

the cavity ABH model with the maximum unit of the grid l_{max} as

$$l_{max} = 220\mu\text{m}\sqrt{100\text{Hz}/f} \tag{1}$$

and the minimum unit of the grid l_{min} is

$$l_{min} = \frac{220\mu\text{m}\sqrt{100\text{Hz}/f}}{6} \tag{2}$$

2.2 Governing equations

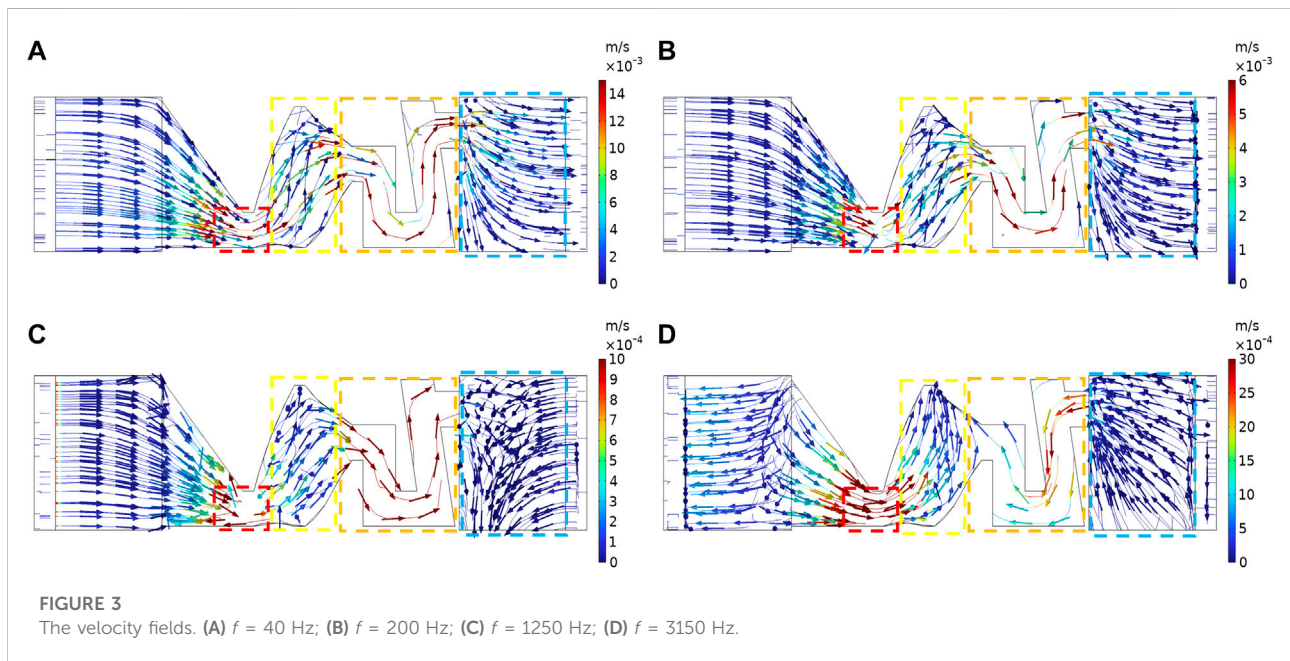
The incident sound waves in the background sound field are

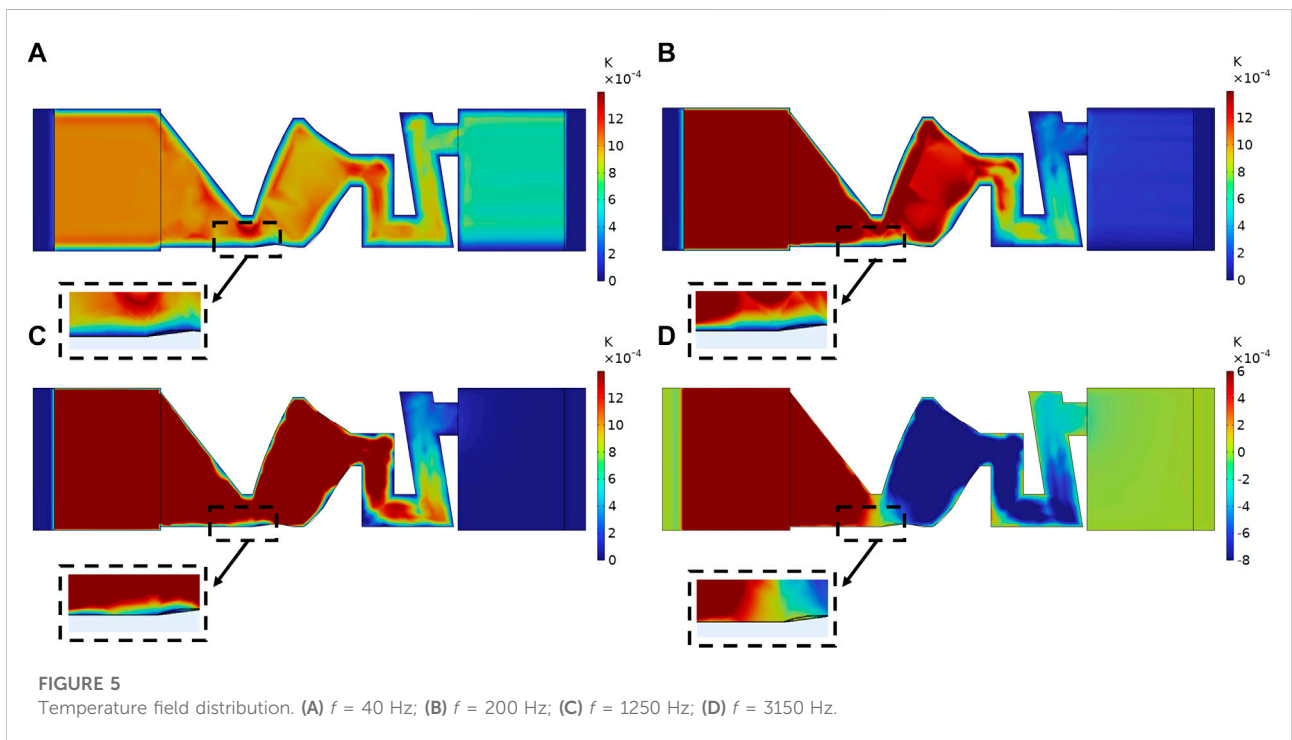
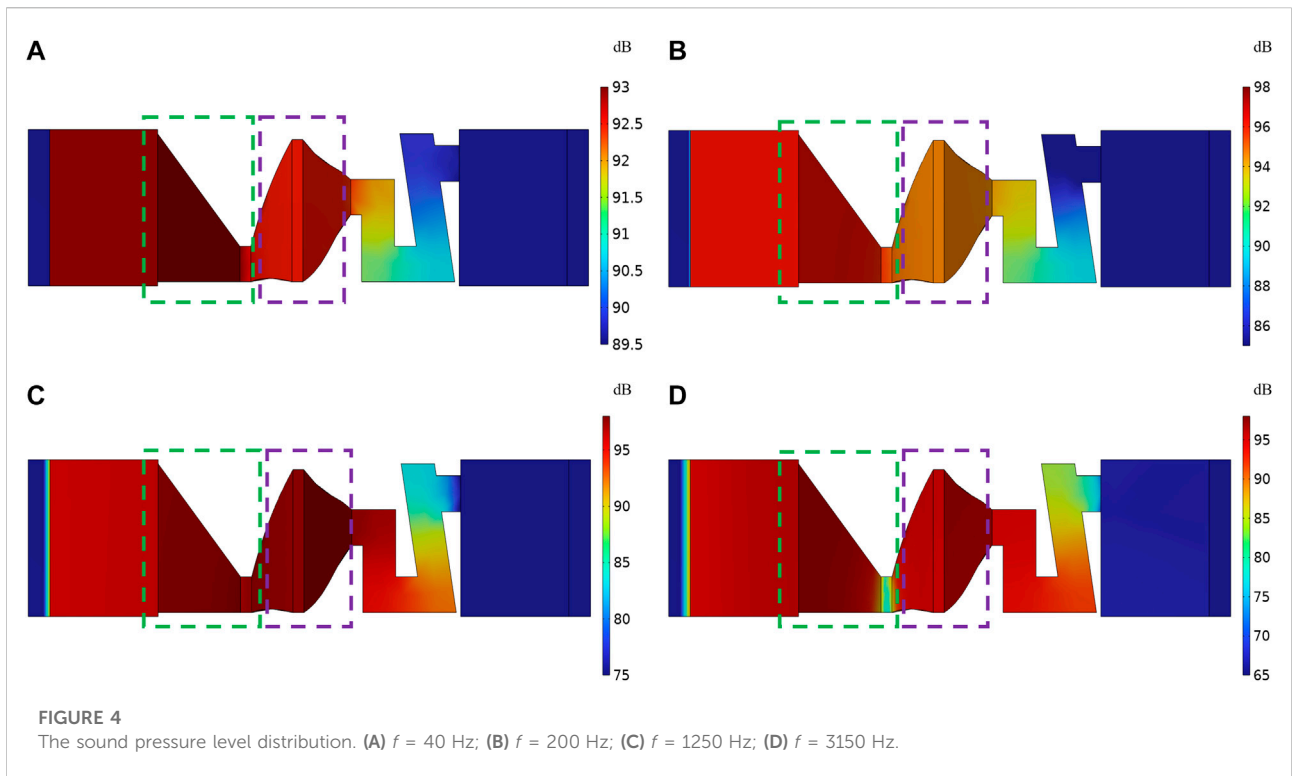
$$p_b = |p_b|e^{-ik_b\vec{n}_k x} \tag{3}$$

$$k_b = \frac{\omega}{c} \left(1 + \frac{i\omega b_{rv}}{\rho_0 c^2} \right)^{-1/2} \tag{4}$$

$$b_{rv} = \frac{4}{3}\mu + \mu_B + \frac{(\gamma - 1)\kappa}{C_p} \tag{5}$$

$$\vec{n}_k = \frac{\vec{e}_k}{|\vec{e}_k|} \tag{6}$$





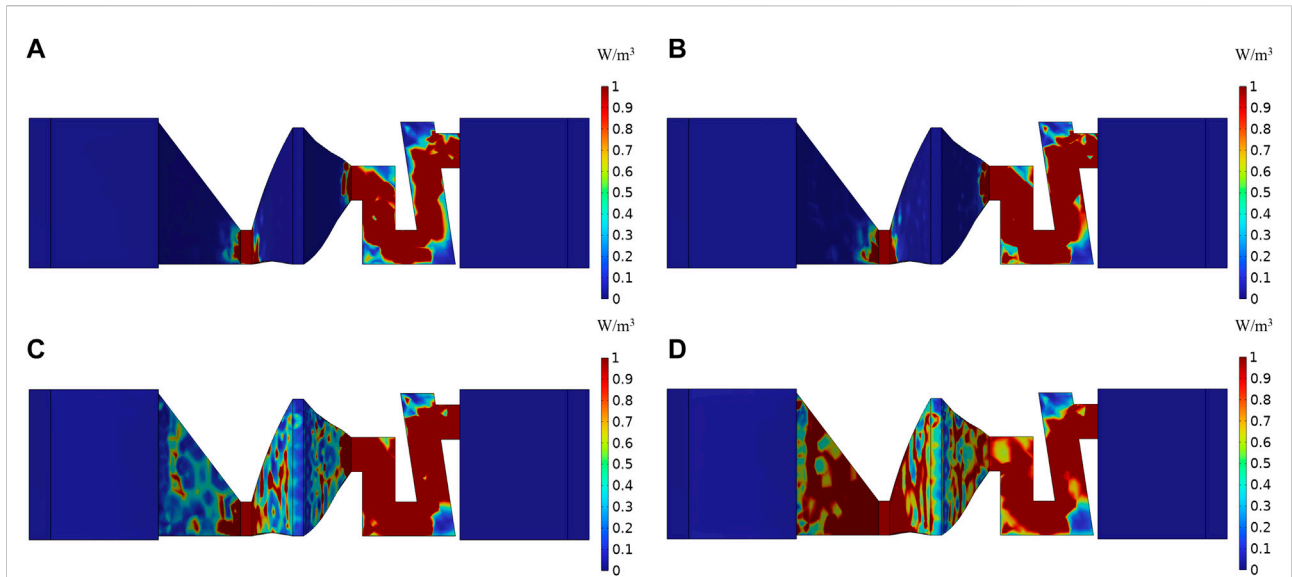


FIGURE 6
 Thermal-power density distribution of the cavity ABH. (A) $f = 40$ Hz; (B) $f = 200$ Hz; (C) $f = 1250$ Hz; (D) $f = 3150$ Hz.

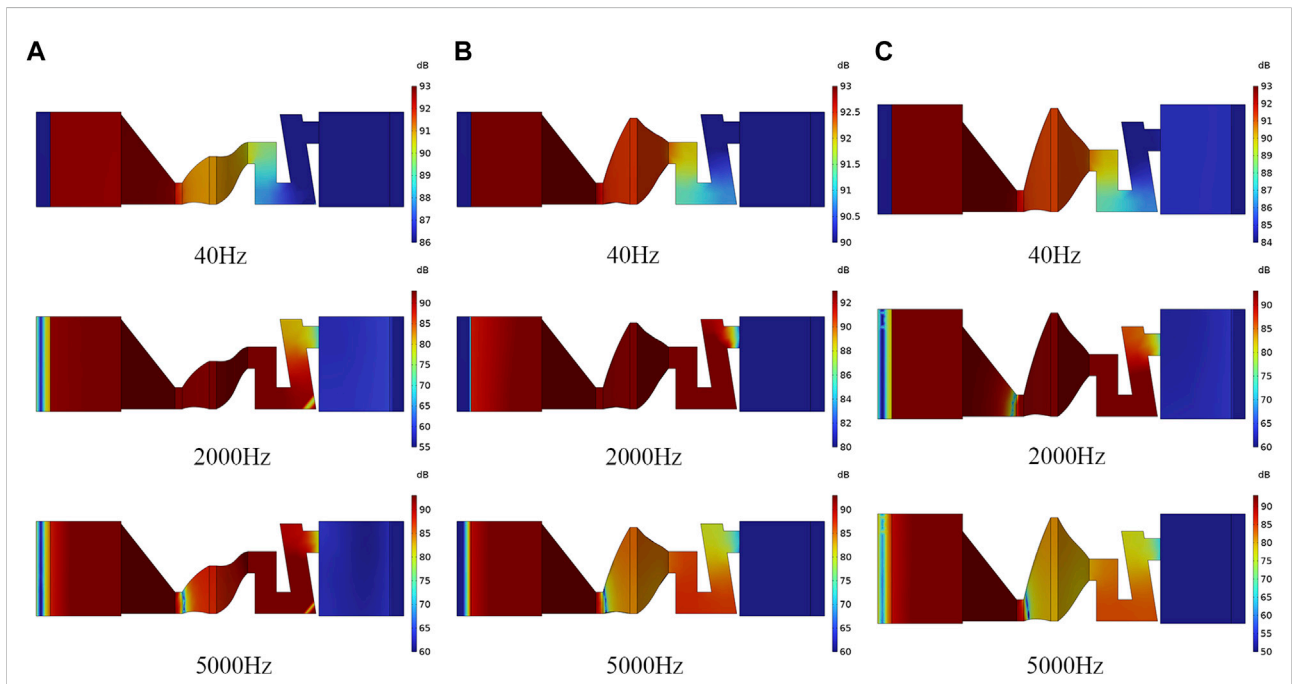


FIGURE 7
 The sound pressure level at different frequencies in different models. (A) Model 1; (B) Model 2; (C) Model 3.

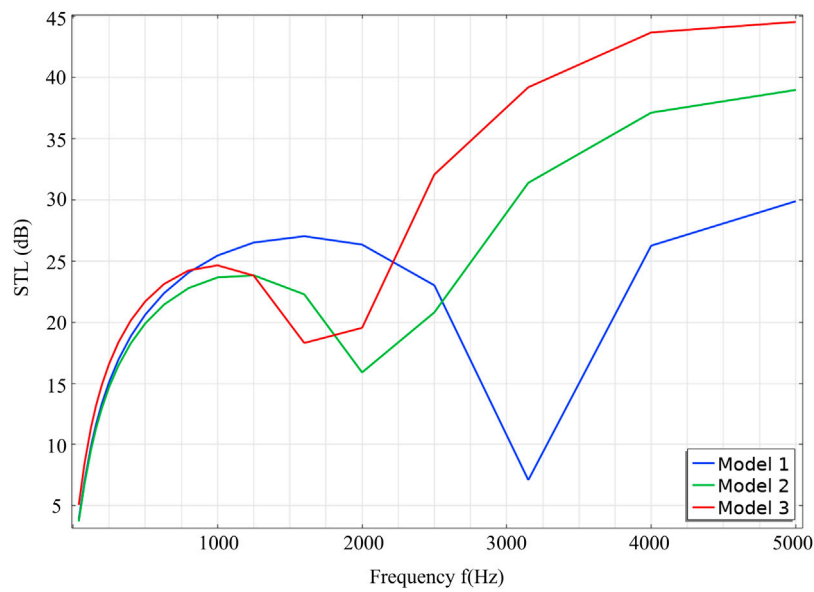


FIGURE 8
The STL of three models.

where $|p_b|$ is the amplitude of the sound pressure, k_b is the wave number of background acoustic field, ω is the frequency of the incident sound wave, c is the sound velocity, μ_B is the bulk viscosity, γ is the ratio of specific heats, κ is the thermal conductivity of the total field, and \vec{e}_k is the wave direction.

The sound pressure in a nonlinear thermos-viscous sound field is

$$p_t = p + p_b \tag{7}$$

where p is the background pressure and $p = 1 \text{ atm}$.

The mass conservation equation in the frequency domain is

$$i\omega\rho_t + \nabla(\rho_0\vec{u}_t) = 0 \tag{8}$$

where ρ_t is the density to be solved, ρ_0 is the initial density, and \vec{u}_t is the velocity to be solved:

$$\rho_t = \rho_0(\beta_T p_t - \alpha_p T_t) \tag{9}$$

$$\beta_T = \frac{1}{\rho_0} \frac{\gamma}{c^2} \tag{10}$$

$$\alpha_p = \frac{1}{c} \sqrt{\frac{C_p(\gamma - 1)}{T_0}} \tag{11}$$

$$\vec{u}_t = \vec{u}_0 + \vec{u}_b \tag{12}$$

where β_T is the coefficient of isothermal compression, α_p is the thermal expansion (isobaric) coefficient, \vec{u}_0 is initial velocity, and $\vec{u}_0 = 0$, \vec{u}_b is the oscillation velocity:

$$\vec{u}_b = \frac{\omega(\beta_T p_b - \alpha_p T_b)}{k_b} \vec{e}_k \tag{13}$$

$$T_b = \frac{i\omega\alpha_p T_0}{i\omega\rho_0 C_p + \kappa k_b^2} p_b \tag{14}$$

where T_b is the temperature to be solved, T_0 is the equilibrium temperature, and $T_0 = 293.15 \text{ K}$.

The momentum equations, which are also Navier–Stokes equations in the frequency domain, can be expressed

$$i\omega\rho_0\vec{u}_t = \nabla\vec{\sigma} \tag{15}$$

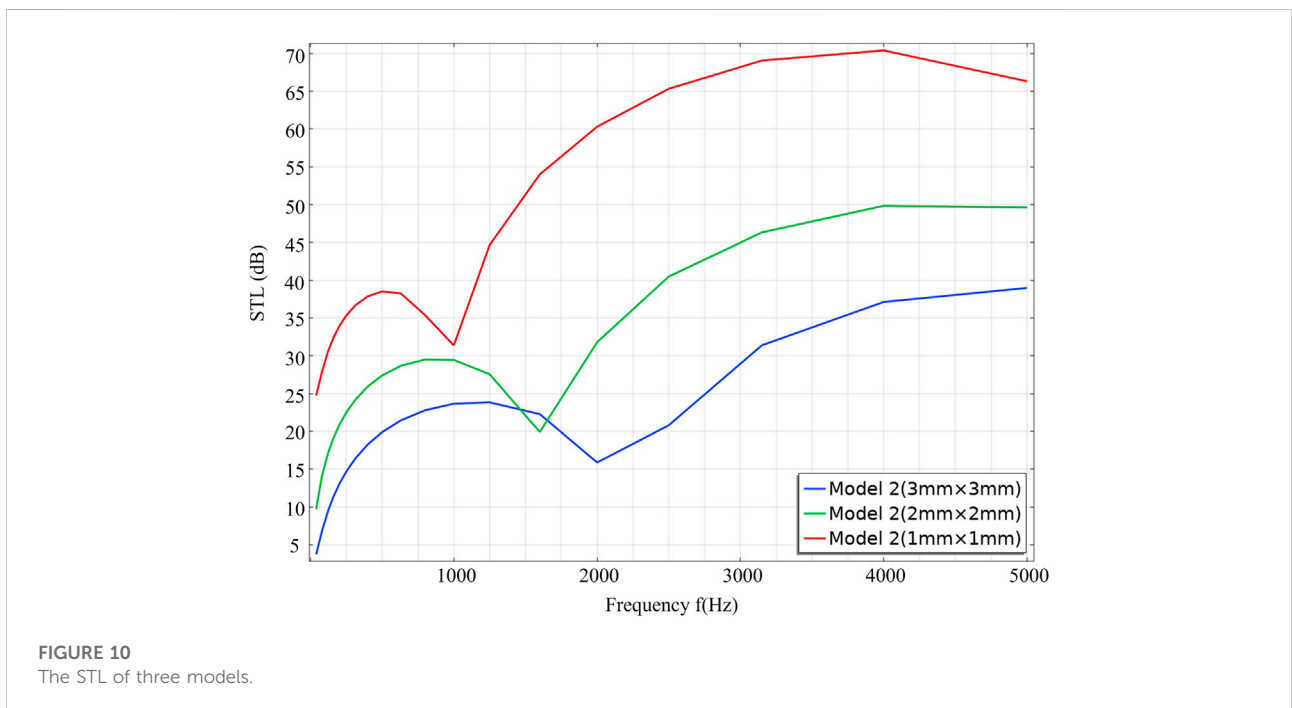
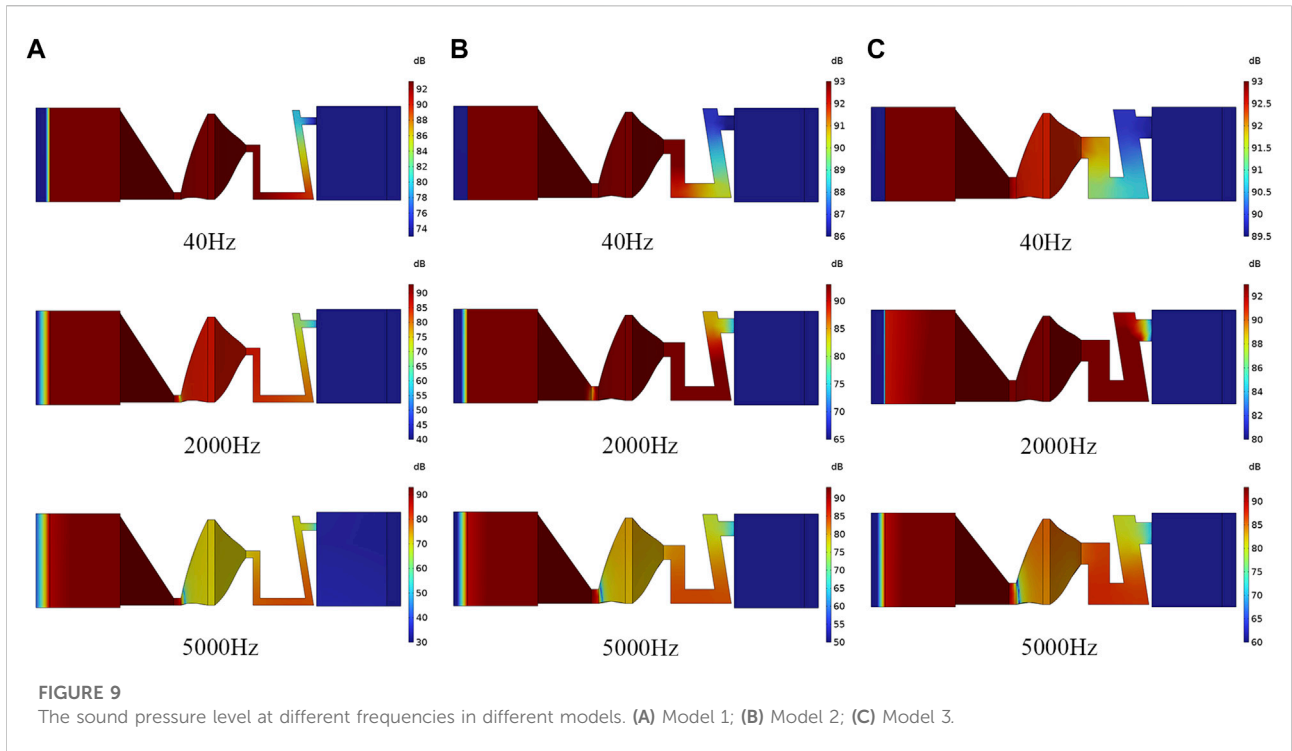
where the term on the right side of Eq. 15 represents the dispersion of the stress tensor and $\vec{\sigma}$ is

$$\vec{\sigma} = -p_t \mathbf{I} + \mu \left(\nabla\vec{u}_t + (\nabla\vec{u}_t)^T \right) - \left(\frac{2}{3}\mu - \mu_B \right) (\nabla\vec{u}_t) \mathbf{I} \tag{16}$$

where \mathbf{I} is the identity matrix. Based on the assumption that small harmonic oscillations have steady-state background properties, the first term on the right of Eq. 16 shows the pressure, and the second and third terms represent the viscous force. For three-dimensional flow field, $\nabla\vec{u}_t$ is expressed as

$$\nabla\vec{u}_t = \begin{bmatrix} \frac{\partial u_x}{\partial x} & \frac{\partial u_x}{\partial y} & \frac{\partial u_x}{\partial z} \\ \frac{\partial u_y}{\partial x} & \frac{\partial u_y}{\partial y} & \frac{\partial u_y}{\partial z} \\ \frac{\partial u_z}{\partial x} & \frac{\partial u_z}{\partial y} & \frac{\partial u_z}{\partial z} \end{bmatrix} \tag{17}$$

The energy conservation equation is



$$\rho_0 C_p \left(i\omega T_t + \vec{u}_t \nabla T_0 \right) - \alpha_p T_0 \left(i\omega \rho_t + \vec{u}_t \nabla \rho_0 \right) = \nabla (\kappa \nabla T_t) + Q \quad (18)$$

where Q is the heat generated by the cavity ABH. Viscous losses occur in the model when there is a gradient within the velocity field, and thermal losses occur when there is a gradient within the temperature field. T_t is the total temperature, and

$$T_t = T_0 + T_b \quad (19)$$

The boundary condition on the wall is

$$\vec{u}_t = 0, T_t = 0 \quad (20)$$

By the above equations, the flow, sound, and temperature fields can be calculated. In Section 3, we will give the detailed simulation results for further analysis.

3 Results and discussions

We obtain the velocity field at different frequencies by calculating the governing equations, as shown in Figure 3. The sound waves propagate to the tip of the cavity at a relatively high speed (see the red dashed box) but decelerate in the cavity (see the yellow dashed box). The waves undergo acceleration and deceleration again as they go through the pipe and out of the ABH (see the orange dashed box and blue dashed box). Meanwhile, it can be observed that the low frequencies waves go through the ABH steadily. When the frequency increases, the motion of the sound waves becomes chaotic (see the yellow and orange dashed box).

The observation of the sound pressure level distribution and the comparison with the velocity field (shown in Figure 4) reveal that the acoustic streaming effects determine sound pressure distribution. Because of the reduction of the tip and pipe section, the sound waves are compressed. This causes an increase in velocity and results in a raise of sound pressure (see the green dashed box). In contrast, the sudden increase in space inside the cavity broadens the distance between each streamline, which decreases the sound pressure (see the purple dashed box in Figures 4A,B). When the waves leave the ABH, they undergo the procession of wave compression and rarefaction for the second time. The low-frequency waves are less affected by ABH because of relatively long wavelengths, which are longer than the length of the ABH. The sound waves can easily pass the ABH, and the sound pressure reduces gradually (see Figures 4A,B). This is how the low-frequency waves go through the ABH. However, as the medium- and high-frequency waves enter the cavity, because of their short wavelength, the nodes of the sound wave are encountered as they travel to the tip (see the green dashed box in Figure 4D). At the same time, the waves are compressed in the cavity, leading

the high sound pressure of the cavity (see the purple dashed box in Figures 4A,B). In the process of the sound wave passing through ABH, its motion is affected, and the sound pressure is also changed. Moreover, the result is that the sound pressure at the exit decreases.

Figure 5 shows the temperature field. We notice an obvious temperature gradient in the ABH (the black dashed box in Figure 5). It is mainly due to the dissipation effect of the boundary layers. Acoustic viscous boundary layers and thermal boundary layers can dissipate acoustic energy in the form of heat. The thickness of the acoustic viscous boundary and the thickness of the thermal boundary layer can be calculated by the following equation:

$$\delta_v = \sqrt{\frac{\mu}{\pi f \rho_0}} \quad (21)$$

where f is frequency, μ is the viscosity coefficient, and ρ_0 is the initial density of the fluid.

$$\delta_t = \sqrt{\frac{\lambda}{\pi f \rho_0 C_p}} \quad (22)$$

where C_p is the heat capacity and λ is the coefficient of thermal conductivity. At 40, 200, 1,250, and 3,150 Hz, the thickness of the viscous boundary layer is 0.346, 0.155, 0.062, and 0.039 mm, respectively. With the decrease in frequency, the layer becomes thicker.

To further explore the acoustic energy dissipation in cavity ABH, we study the density of thermal-power consumption. Figure 6 shows that, at low frequencies, the thickness of the thermal viscous layer is relatively thick at the boundary and part of the energy is dissipated by the layer (shown in Figures 6A,B). The thermal consumption is mainly situated at a small scale. As the frequency increases, the thermal viscous layer becomes thinner, dissipating less acoustic energy. The thermal-power consumption is distributed in all the ABH (Figures 6C,D).

Through learning, we find that the cavity with a sudden change area can alter the velocity in the cavity and then influence the change of sound pressure. To deeply investigate this characteristic, we propose three models, changing the largest area of the cavity and observing the effect of the area change. The largest areas of Model 1, Model 2, and Model 3 are 6.8×15.2 mm, 12.2×22.9 mm, and 14.6×27.4 mm, respectively.

Figure 7 is the sound pressure level at different frequencies of three cavity ABHs. The sound waves of 40 Hz are less influenced by the ABH, which causes a small drop in sound pressure. While the sound waves of 2,000 Hz can be located in the cavity, the sound waves of 5,000 Hz are clustered at the tip, resulting in a decrease in the sound pressure at the exit. By contrasting the three models, we notice that Model 3 has a greater decrease in the sound

pressure in the cavity at high frequencies, as shown in Figure 7C.

We calculate the STL and show the result of three models in Figure 8. The STL can be defined as

$$STL = 20 \lg\left(\frac{P_{in}}{P_{out}}\right) = 10 \lg\left(\frac{P_{in}}{P_{out}}\right)^2 \quad (23)$$

where P_{in} and P_{out} represent the incoming power at the entrance and the outgoing power at the exit.

The three curves are almost the same at low frequencies, which supports the conclusion that the area change of the cavity has a small influence on the low-frequency waves and no improvement in sound insulation at low frequencies. However, the motion of the sound waves with high frequencies is affected more, so the sound pressure drops more at the exit of ABH. This illuminates that increasing the cross section of the cavity lead to better sound insulation at high frequencies.

We also notice that the tip and the pipe of ABH can effectively insulate the sound waves. Therefore, we change the cross section of the hole and pipe. The areas of small scale in the three models are 1×1 mm, 2×2 mm, and 3×3 mm, respectively.

Figures 9, 10 show the sound pressure level at different frequencies and the STL of three models. As shown in Figure 9, with the reduction in the tip and pipe's cross-sectional area, the sound pressure drops more at each frequency. Besides, the smaller cross section of the tip can also easily focus the high-frequency sound waves on the tip (shown in Figure 9 at 2,000 and 5,000 Hz). In Figure 10, we can observe that reducing the cross-sectional area of the tip and the pipe can improve the sound insulation effect of the whole frequency band. In the low-frequency band, as the side length is reduced from 3 to 1 mm, STL can be increased by about 20 dB. The sound insulation effect is more significant in the frequency band exceeding 2,000 Hz.

4 Conclusion

We propose a theoretical model of cavity ABH to investigate its acoustic streaming effects. The flow, sound, and temperature fields at different frequencies are obtained by governing equations.

From the comparison of the velocity field and the sound pressure level field, it can be seen that the velocity field is closely related to the sound pressure level field, and the reduced cross section causes an increase in velocity, resulting in an increase in sound pressure. On the contrary, the decrease in speed caused by the enlarged

cross-section causes a decrease in sound pressure. Thus, we conclude that the sound flow effect determines the sound pressure distribution. In addition, when we study the temperature field, we find that there is an obvious temperature gradient, which is mainly caused by the dissipation effect of the thermal viscous boundary layer.

At the same time, combined with the closely related characteristics of sound flow effect and sound pressure, we propose methods to improve the sound insulation effect. The first is to increase the area of cross section in the cavity, which can improve the isolation of high-frequency sound waves. The second is to reduce the cross-sectional area of the small size, which can better isolate the sound waves in the full frequency band. This provides new ideas for low-frequency sound insulation.

Data availability statement

The original contributions presented in the study are included in the article/Supplementary Material. Further inquiries can be directed to the corresponding authors.

Author contributions

Conception and design: XL, MH, and JC; analysis and/or interpretation of data: SW, JC, HL and DL; drafting the manuscript: XL and MH; revising the manuscript critically for important intellectual content: XL and YZ.

Conflict of interest

Author XH is employed by Jianglu Electromechanical group Co., Ltd.

The remaining authors declare that the research was conducted in the absence of any commercial or financial relationships that could be construed as a potential conflict of interest.

Publisher's note

All claims expressed in this article are solely those of the authors and do not necessarily represent those of their affiliated organizations or those of the publisher, the editors, and the reviewers. Any product that may be evaluated in this article, or claim that may be made by its manufacturer, is not guaranteed or endorsed by the publisher.

References

- Denis, V., Pelat, A., and Gautier, F. (2016). Scattering effects induced by imperfections on an acoustic black hole placed at a structural waveguide termination. *J. Sound Vib.* 362, 56–71. doi:10.1016/j.jsv.2015.10.016
- Denis, V., Pelat, A., Touzé, C., and Gautier, F. (2017). Improvement of the acoustic black hole effect by using energy transfer due to geometric nonlinearity. *Int. J. Non-Linear Mech.* 94, 134–145. doi:10.1016/j.ijnonlinmec.2016.11.012
- Ei-Ouahabi, A., Krylov, V. V., and O'Boy, D. (2015). "Investigation of the acoustic black hole termination for sound waves propagating in cylindrical waveguides," in *Proceedings of the inter-noise and noise-con congress and conference* (San Francisco, USA: Institute of Noise Control Engineering).
- Ei-Ouahabi, A., Krylove, V. V., and O'Boy, D. (2015). "Experimental investigation of the acoustic black hole for sound absorption in air," in *Proceedings of 22nd international congress on sound and vibration* (Florence, Italy).
- Gao, N., Guo, X., Deng, J., Cheng, B., and Hou, H. (2021). Elastic wave modulation of double-leaf ABH beam embedded mass oscillator. *Appl. Acoust.* 173, 107694. doi:10.1016/j.apacoust.2020.107694
- Gao, N., and Lu, K. (2020). An underwater metamaterial for broadband acoustic absorption at low frequency. *Appl. Acoust.* 169, 107500. doi:10.1016/j.apacoust.2020.107500
- Gao, N., Luo, D., Cheng, B., and Hou, H. (2020). Teaching-learning-based optimization of a composite metastructure in the 0-10 kHz broadband sound absorption range. *J. Acoust. Soc. Am.* 148, EL125–EL129. doi:10.1121/10.0001678
- Gao, N., Wang, B., Lu, K., and Hou, H. (2021). Complex band structure and evanescent Bloch wave propagation of periodic nested acoustic black hole phononic structure. *Appl. Acoust.* 177, 107906. doi:10.1016/j.apacoust.2020.107906
- Gao, N., Wei, Z., Hou, H., and Krushynska, A. O. (2019). Design and experimental investigation of V-folded beams with acoustic black hole indentations. *J. Acoust. Soc. Am.* 145, EL79–EL83. doi:10.1121/1.5088027
- Gao, N., Zhang, Z., Deng, J., Guo, X., Cheng, B., and Hou, H. (2022). Acoustic metamaterials for noise reduction: A review. *Adv. Mater. Technol.* 7, 2100698. doi:10.1002/admt.202100698
- Li, H., Sécail-Géraud, M., and Pelat, A. (2021). Experimental evidence of energy transfer and vibration mitigation in a vibro-impact acoustic black hole[J]. *Appl. Acoust.* 182, 1–5. doi:10.1016/j.apacoust.2021.108168
- Li, H., Touzé, C., and Pelat, A. (2019). A vibro-impact acoustic black hole for passive damping of flexuralbeam vibrations[J]. *J. Sound Vib.* 450, 28–46. doi:10.1016/j.jsv.2019.03.004
- Liang, X., Chu, J., Tan, J., Nie, S., and Liu, B. (2021). Spontaneous catastrophe behaviour in acoustic black holes at low frequencies. *Appl. Acoust.* 180, 108109. doi:10.1016/j.apacoust.2021.108109
- Liang, X., Chu, J., Zhou, Z., Hu, C., Peng, J., Liu, B., et al. (2022). Turbulence in cavity acoustic black hole[J]. *Mech. Syst. Signal Process.* 165, 108303. doi:10.1016/j.ymsp.2021.108303
- Liang, X., Wang, S., Liu, M., Nie, S., Peng, J., Zhou, Z., et al. (2021). Study on low frequency sound insulation characteristic of thin acoustic black hole. *Mod. Phys. Lett. B* 35, 2150198. doi:10.1142/s0217984921501980
- Liang, X., Zhou, Z., and Wu, J. H. (2019). The experimental study on low frequency sound transmission characteristics of the acoustic black hole[J]. *Mod. Phys. Lett. B* 33 (6), 1950458. doi:10.1142/s021798491950458x
- Ma, F., Huang, Z., Liu, C., and Wu, J. H. (2022). Acoustic focusing and imaging via phononic crystal and acoustic metamaterials. *J. Appl. Phys.* 131, 011103. doi:10.1063/5.0074503
- Ma, F., Wang, C., Liu, C., and Wu, J. H. (2021). Structural designs, principles, and applications of thin-walled membrane and plate-type acoustic/elastic metamaterials. *J. Appl. Phys.* 129, 231103. doi:10.1063/5.0042132
- Mi, Y., Zhai, W., Cheng, L., Xi, C., and Yu, X. (2021). Wave trapping by acoustic black hole: Simultaneous reduction of sound reflection and transmission. *Appl. Phys. Lett.* 118, 114101. doi:10.1063/5.0042514
- Mironov, M. A. (1988). Propagation of a flexural wave in a plate whose thickness decreases smoothly to zero in a finite interval. *Sov. Phys. Acoust.* 34 (3), 318–319.
- Mironov, M., and Pisyakov, V. (2002). One-dimensional acoustic waves in retarding structures with propagation velocity tending to zero. *Acoust. Phys.* 48, 347–352. doi:10.1134/1.1478121
- Mironov, M., and Pisyakov, V. (2020). One-dimensional sonic black holes: Exact analytical solution and experiments. *J. Sound Vib.* 473, 115223. doi:10.1016/j.jsv.2020.115223
- Zhang, X., and Cheng, L. (2021). Broadband and low frequency sound absorption by Sonic black holes with Micro-perforated boundaries. *J. Sound Vib.* 512, 116401. doi:10.1016/j.jsv.2021.116401